Analysis of deformation of levee caused by large diameter shield tunneling in river crossing tunnel

LU Zhongxiang[1], SHOU Lingchao[2], Rini Asnida Abdullah[1], Muhammad Irfan Bin Shahrin[1], CHEN Yintao[1], SHAO Xin[3], FAN Wenju[4], Amber Islam[1], ZHANG Hengxu[5]

1 Universiti Teknologi Malaysia

2 Zhejiang Mingsui Technology Co.Ltd

3 Zhejiang Academy of Transportation Science

4 Ningxia Institute of Science and Technology

5 China Railway 14th Bureau Group Corporation Limited

Abstract

This study utilizes ABAQUS finite element software to analyze embankment deformation during shield tunneling. Results reveal that shield tunneling effects are manageable.The left tunnel line successfully tunnels beneath the embankment, causing a maximum settlement of 8.7 mm, meeting regulations. The ground surface exhibits a "V"-shaped lateral settlement trough, approximately five times the tunnel centerline width. Conversely, the right tunnel line induces a more extensive impact, with a 12.2 mm maximum settlement.Different lateral settlement patterns emerge in soil at varying depths. The left tunnel creates a "V" shape, with slightly increasing settlement above the tunnel axis as depth increases, accompanied by narrower troughs. The right tunnel line results in a pronounced "W" shape, especially at the grouting layer depth.Horizontal displacement forms an "S" shape, with maximum displacement at positions ±i from the tunnel axis. The right tunnel line induces greater maximum horizontal displacement than the left.In summary, this numerical analysis provides insights into embankment deformation during shield tunneling, aiding in assessing the impact and guiding safe tunneling beneath embankments.

1. Introduction

With the rapid development of urban transportation, the number and scale of urban cross-river tunnel constructions are also expanding. These tunnels, primarily built using large-diameter mud shield methods, have seen their outer diameters grow from approximately 11 metersto about 15 meters [1,2]. Notably, these river-crossing tunnels must traverse through river embankments, inevitably causing soil disturbance, particularly during the construction of super-large diameter mud shield tunnels. Given the intricacy of embankment structures and the vital role that river embankments play in safeguarding the lives and property of communities on both sides of the river, it becomes crucial to adopt rational construction parameters and measures. This approach aims to minimize the impact of shield tunneling on embankment structures.

In recent years, the engineering field has accumulated significant experience regarding the disruptive effects of shield tunneling through levees. Zhang et al. employed finite-difference software to construct a three-dimensional numerical model of the Nanjing Weisan Road super-diameter shield tunnel, which crosses the Yangtze River embankment. They calculated the settlement pattern and overall stability of the embankment [3]. Building upon the context of the Chengjiang West Road tunnel in Jiangyin, Han Lei et al. employed the

displacement control finite element method, which is based on the formation loss rate, to compute the embankment settlement under various formation loss rates. They also proposed recommendations for control [4]. Utilizing monitoring data and the Peck empirical formula, Li and Huang examined the disruption and settlement patterns of the Qiantang River levee during the shield crossing construction of the Qingchun Road Tunnel in Hangzhou City [5]. They also suggested settlement control measures for the mud shield crossing the levee [5,6]. Wu et al. utilized the FLAC3D finite difference program in conjunction with field measurements to compute and analyze the deformation patterns of the levee resulting from the penetration of the Qiantang River levee by the mud-water balanced shield, which has a diameter of 11.68m [7]. Their study revealed that the transverse settling trough at the top of the levee resembled that of a subway shield with a diameter of 6.34m, displaying a Gaussian normal distribution. The Peck formula remains applicable for estimating settlement; however, the change in settlement volume and trough width with depth is not as pronounced as observed with the 6.34m diameter subway shield. Huang Hai investigated the surface settlement of the embankment caused by large-diameter shield tunneling under the Qiantang River. The study revealed that the transverse settlement trough of the levee generally follows a normal distribution pattern, with the greatest settlement occurring at the center of the tunnel axis. Settlement diminishes gradually as distance from the tunnel center increases, and

settlement distribution along the tunnel axis is symmetrical, in line with the normal distribution curve proposed by Huang [8]. Relying on the Jilou Road Tunnel project, Zhu et al. analyzed the settlement patterns and characteristics of the large embankment section during the shield tunneling process through the levee using field-measured data. They employed a detailed dynamic simulation of the shield tunnel driving process and observed that the initial settlement rate of the large embankment section during the shield tail ejection stage was greater and more susceptible to disturbance compared to that of an ordinary flat section [9]. Moreover, the top of the levee is particularly sensitive to the disturbance caused by deep soil. Xie et al. utilized finite element software to construct a three-dimensional numerical model for the super-diameter shield tunneling across the Yangtze River levee [10]. They conducted a detailed simulation of the construction process, considering construction elements such as soil excavation, mud-water support, segment lining, grouting behind the wall, and formation loss. Lin et al. based their study on the Liuyang River levee engineering section of Changsha Metro Line 6, They investigated the deformation of the levee under shield tunnel excavation conditions [11]. Wu et al. analyzed the risk factors associated with mud shield tunneling through levee engineering [12]. They examined the causes, hazards, and avoidance measures of these risks and validated the effectiveness of the risk control measures by referencing the engineering example of mud shield tunneling through the levee in the Qingchun Road Tunnel in Hangzhou. Tamir et al. simplified the modeling of the tunnel boring machine shield while incorporating the hardened soil constitutive model [13]. This approach enabled them to capture crucial aspects of the shield tunneling process, such as joint segment lining, grouting pressure, time-varying grout hardening, and nonlinear soil behavior. Hyobum et al. conducted laboratory pressure blade shear tests to examine the rheological properties of sandy soils under foam conditions [14]. They investigated how varying water content, foam injection ratio (FIR), and confining pressure affected the rheological properties of soil under foam conditions. Milad et al. utilized the finite element limit analysis method to assess the limit support pressure in undrained clay [15]. Their evaluation considered horizontal pseudo-static seismic forces directed outward from the face. Zdenek et al. presented a new approach for incorporating the formation process into the analysis of pressure transfer [16,17]. This method was specifically designed for shallow slurry penetration depths smaller than the cutting depth of the tools. Hoonil et al. reported on the significant ground subsidence that ensued after the structural deformation of tunnel segments during the excavation of a cross-passage between two main tunnels [18]. These main tunnels were excavated by an earth pressure balance shielded tunnel boring machine (EPB shield TBM) and were constructed in the deltaic region near the Nak-Dong River in Korea.

Most of the existing research focuses on the analysis of levee settlement, with few studies addressing the settlement and horizontal displacement characteristics of deep soil in levees. Therefore, analyzing the three-dimensional deformation characteristics of levees after shield tunneling is beneficial for understanding the patterns and managing construction risks. In this paper, the deformation (settlement and displacement) of the levee caused by the large-diameter shield machine during the construction of the Jiangshan Road tunnel in Hangzhou is numerically calculated, and the three-dimensional deformation characteristics of the levee are studied.

2. Project overview and geological conditions

2.1 Project overview

The Genshandong Road Cross-River Tunnel is a significant infrastructure project situated between the Xisha Bridge and Jiangdong Bridge, spanning a total length of 4462.26m. This tunnel plays a vital role in the region's transportation network, and its technical aspects are noteworthy for a comprehensive understanding. This shield tunnel features a single-layer lining with segment assembly. It boasts an impressive outer diameter of 14.5m, an inner diameter of 13.3m, a segment thickness of 0.6m, and a ring width of 2m. The tunnel comprises 10 "9+1" sections, and these sections are assembled with staggered joints, tightly secured by high-strength bolts. The construction of the shield tunnel, a significant infrastructure project in the region, begins at the eastern starting well of the Big River and proceeds westward, reaching its destination at the Xisha receiving well. However, the tunnel faces a major challenge when it crosses the mighty Qiantang River due to the high deformation requirements of the levee caused by tidal influence. For a visual representation of the current status of the levee, as shown in Figure 1.
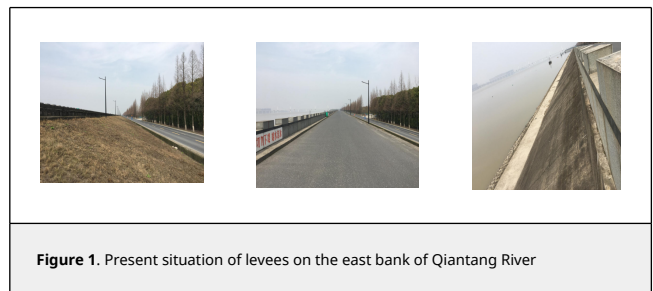

Figure 1. Present situation of levees on the east bank of Qiantang River

2.2 Hydrogeological conditions and monitoring arrangement

The shield tunnel passes through various soil layers, including sandy silt, silt, silty clay, mucky clay, clay, Fully weathered rock, and Moderately weathered rock. Despite the levee not being strengthened before shield construction, strategic monitoring points were installed on the levee to ensure safety. These measures are crucial for maintaining project stability and safety. For detailed information about the tunnel's soil layers and monitoring setup, as shown in Figure 2.
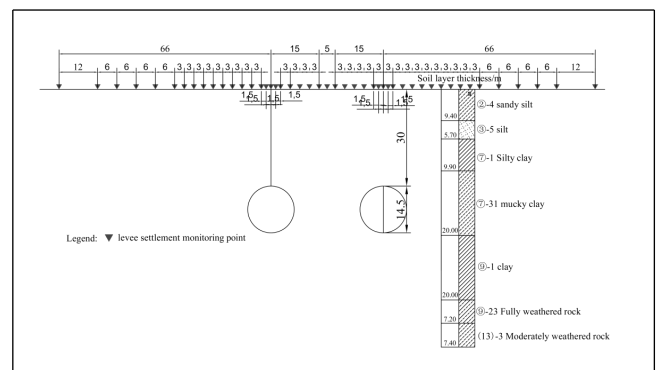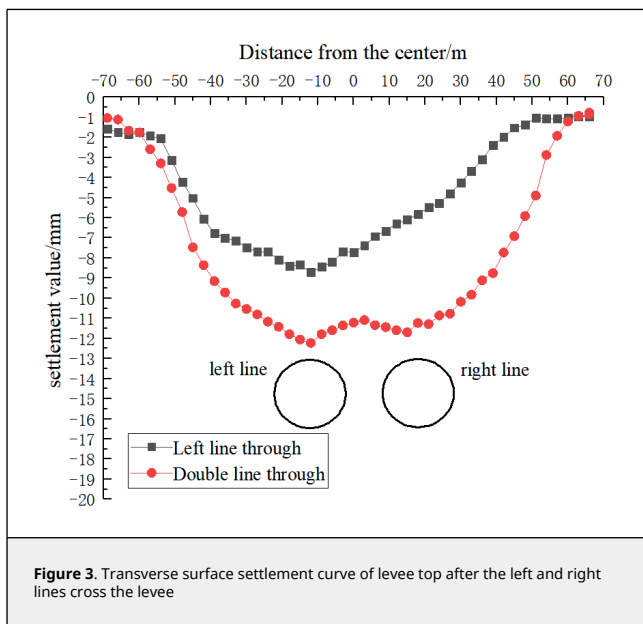

Figure 2. Monitoring site layout profile

3. Measured analysis of surface settlement of levees

3.1 Lateral surface settlement of levee top

In Figure 3, we observe the settlement patterns above and around the tunnel axis. The most significant settlement occurs directly above the tunnel axis. For the left-line shield tunnel, the transverse surface settlement generally forms a "V" shape distribution, with a maximum settlement of 8.7mm directly above the left line.

Conversely, after the right-line shield tunnel crosses the levee, the transverse surface settlement generally exhibits a "W" shape distribution. The maximum settlement reaches 12.2mm, which is still directly above the left line of the shield tunnel and greater than the surface settlement above the right line. Additionally, the settlement in the middle of the left and right lines is slightly less than the settlement value above the tunnel.

Figure 3. Transverse surface settlement curve of levee top after the left and right lines cross the levee

For the prediction of ground displacement caused by single-line tunnel excavation, the horizontal distribution estimation formula of ground settlement proposed by Peck is generally adopted in current engineering practice [19]:

$$S(x) = S_{max}\exp\left(-\frac{x^2}{2i^2}\right) \tag{1}$$

$$S_{max} = \frac{V_s}{i\sqrt{2\pi}} = \frac{\pi R^2 \eta}{i\sqrt{2\pi}} \tag{2}$$

where $S(x)$ is the ground subsidence caused by ground loss; x the distance from the tunnel center line; S_{max} the maximum settlement caused by the formation loss at the center line of the tunnel; i the width coefficient of surface settling trough; V_s the stratum loss per unit length of tunnel; η the formation loss rate, is the ratio of the surface subsidence trough area to the tunnel excavation area; and R is the radius of tunnel excavation.

When the Peck formula is used to predict the transverse surface settlement, the most important thing is to determine the formation loss rate V_1 and the width coefficient of sedimentation tank i. O'Reilly and New [20] proposed the following values in accordance with the experience of London:

$$i = Kz_0 \tag{3}$$

where K is the sedimentation tank width parameter; and z_0 the buried depth for the tunnel axis.

In the paper, the Peck formula is utilized to fit the measured transverse surface settlement curve of the embankment top after the left line crosses the embankment. This analysis aims to compare the surface settlement of the embankment top and evaluate the applicability of the Peck formula in the project, as shown in Figure 4. The findings from this analysis are crucial for understanding the behavior of the embankment top and its response to the tunneling process.

Figure 4. Comparison between the measured value of land surface settlement and the Peck fitting value
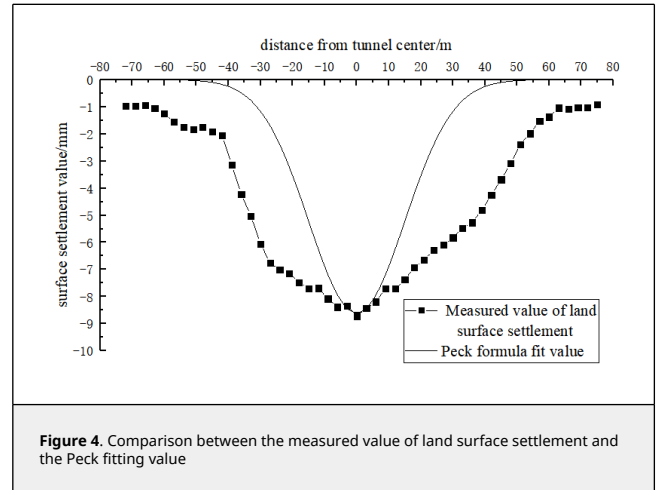
Upon analyzing Figure 4, we observe that the variation in the surface settlement curve closely aligns with the Peck formula. However, it's noteworthy that the measured values in the field are slightly larger than those fitted by the Peck formula. The discrepancy in measured values may arise due to the greater structural weight of the levee compared to typical strata. This difference is reflected in the higher soil and water pressure, as well as settlement, beneath the levee excavation surface at the same burial depth compared to shield tunneling in other general strata. The large diameter of the shield used influences these factors. Despite the challenges posed by large-diameter shield tunnels, the Peck formula remains applicable, allowing engineers to predict the distribution of transverse settling troughs at the top of the levee. These predictions, which consider factors such as formation loss (Vs) and the width coefficient of the settling trough (i), are invaluable for assessing and managing levee settlement and deformation during construction.

3.2 Surface settlement of shield through various stages

These stages provide a framework for understanding the settlement process during shield tunnel construction and are crucial for monitoring and managing potential impacts on surrounding structures.

1. The shield approaches: the shield excavation face has not reached the monitoring section, and the distance is about 2 times the diameter of the shield.
2. The shield arrives: the excavation face of the shield has not reached the monitoring section, and the distance is 0~2 times the diameter of the shield.
3. The shield goes through: when the shield excavation face passes through the monitoring section, the distance is 1 times the diameter of the shield.
4. The shield leaves: when the shield excavation face leaves

the monitoring section about 1 times the diameter of the shield.

5. Final stable times: about 10 times the diameter of the shield when the shield excavation face leaves the monitoring section.

As shown in Figure 5, this is the lateral surface settlement curve of the levee at each stage of left-line shield construction. By comparing these curves, it can be observed that as the shield advances, surface settlement gradually increases. The width of the transverse settlement trough in the same section remains relatively constant, and the settlement curve becomes steeper. When the shield reaches the monitoring fault front (approximately 1D~2D away from the section, D: the tunnel diameter), a noticeable transverse settlement trough with a width of about 15~20 meters is generated. The maximum land settlement occurs at the center of the tunnel, with settlement decreasing as one moves farther away from the tunnel center.
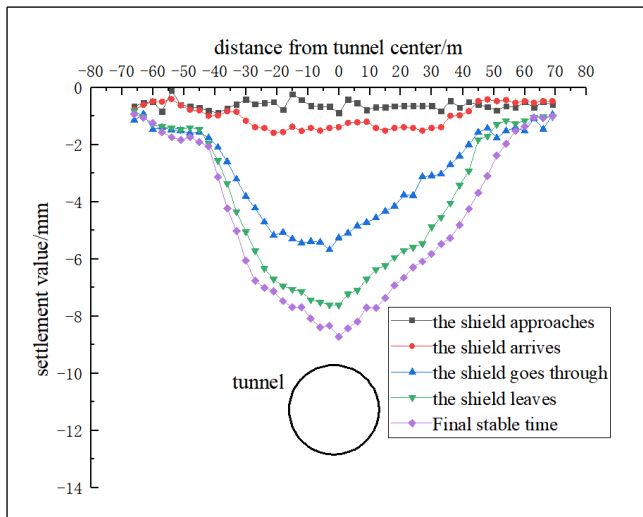

Figure 5. Surface settlement curve of the left line shield crossing the levee at each stage

Table 1 provides the percentage distribution of settlement in different stages of shield tunnel excavation. In the early settlement stage of the monitoring point, the settlement value accounts for 7% of the total settlement, which, while relatively small, should not be overlooked. Moving on to the arrival stage of the shield, we see that it contributes 14% of the total settlement. However, the phases of shield passage and post-shield passage are particularly critical, with these two stages contributing to a larger proportion of the total settlement, specifically 43% and 23%, respectively. In fact, settlements in these stages collectively account for approximately 66% of the total settlement value, making this phase the most concerning due to its rapid and substantial settlement changes. Finally, the late sedimentation stage produces around 13% of the total settlement value. To summarize, the percentage of settlement in various stages of shield tunnel excavation varies significantly. The early and late stages contribute relatively small percentages, while the arrival stage accounts for 14% of the total settlement. However, it's during the phases of shield passage and post-shield passage that settlement percentages are most substantial, combining to make up approximately 66% of the total settlement value. This phase is of particular concern due to its rapid and pronounced settlement changes.

Table 1. Percentage of the total settlement at each stage of the monitoring point (%)

Pre-arrival settlement of shield	Phase settlement of shield arrival	Phase settlement of the shield as it passes through	Phase settlement after shield passage	Long-term subsequent stage settlement
7	14	43	23	13

4. Numerical analysis of levee deformation

To gain insights into the soil deformation characteristics of the levee during sequential passage by the left and right-line shields, we conducted an investigation using the advanced finite element software ABAQUS. This analysis aims to calculate and compare the dynamic construction processes of the shields to understand how they impact the soil and the overall construction of the tunnel.

4.1 Numerical calculation model

To gain a comprehensive understanding of the real-world engineering scenario and design parameters, we have developed a numerical calculation model using ABAQUS finite element software. This model is designed to simulate the effects of the shield tunnel's construction, which comprises two parallel lines with a centerline separation of 35m. One of the key features of the model is its representation of the grouting filler within the shield tunnel gap as a uniform and equally thick grouting layer.

In our simulation, we have incorporated the thrust generated by the shield machine and the pressure exerted by cement in the form of nodal concentrated forces. Our model encompasses various elements, including the surrounding rock, pipe segments, grouting material, and the levees, all represented using solid elements.

The numerical model's dimensions are as follows: a longitudinal length of 56m, a transverse width of 180m, and a vertical height ranging from 76.1m to 84.6m. This extensive model is divided into 140,208 units and comprises 148,071 nodes, ensuring a comprehensive representation of the system. For a visual representation, as shown in Figure 6.
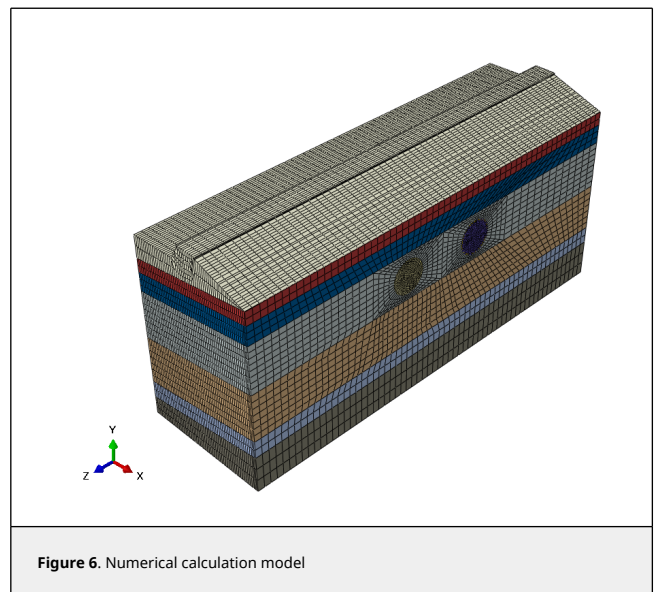

Figure 6. Numerical calculation model

In shield construction, a ring gap will be formed between the tunnel excavation wall and the outer ring of the segment when the segment is detached from the shield tail. If the action of grouting and pressure is ignored, the soil mass will move to this gap and produce a large displacement.In the actual grouting process, the slurry fills the gap of the shield tail and penetrates

into the soil body, and then gradually hardens. If the hardening of the grouting material is not considered, the settlement value will also deviate from the actual value by using the isogeneration layer simulation. Because the interaction of shield tail grouting will form a mixture of soil and cement slurry, the grouting layer can be simulated by elastic model, and the hardening of grouting material can be simulated by the variable stiffness of grouting material [21]. And an elastic model is utilized for soil. The specific material parameters for these models are detailed in Table 2.

Table 2. Material parameters of the model

Material name	Weight (kN/m³)	Cohesion (kPa)	Internal friction Angle (°)	Poisson's ratio	Elastic modulus (MPa)
Sandy silt	19.8	12	32	0.2	19
Silt	19.9	13.5	33.4	0.22	20
Silty clay	17.6	19	32	0.25	8
Mucky clay	18.4	27	34	0.35	4
Clay	19.6	45	17.3	0.36	9
Fully weathered rock	22.3	50	22	0.26	320
Moderately weathered rock	22.6	200	22	0.23	550
Grouting layer	21	-	-	0.2	15
Segment	25	-	-	0.17	34500

The boundary conditions and deformation constraints are crucial for accurately representing the real-world scenario in our simulation. To achieve this, we have implemented free boundaries at the top and surface of the levee to allow unrestricted movement. This setup enables us to capture the natural behavior of the levee's surface under various loading conditions. Around the levee, we have applied deformation constraints to account for the complex interactions that occur in this region. These constraints help us model the interaction between the levee and its surroundings more accurately. Additionally, at the bottom surface, we have limited deformation in the X, Y, and Z directions to reflect the response of the ground to the construction process. This ensures that our simulation captures the realistic behavior of the ground beneath the levee. Furthermore, we have introduced lateral constraints on the sides of the model to account for the lateral support provided by the surrounding soil. These constraints play a crucial role in simulating the lateral stability of the levee under different loading conditions.

4.2 Simulation of shield excavation process

To simulate the step excavation process of the shield accurately, we utilize the element life and death function to manage the elements representing the shield machine, the grouting layer, and the segment. This process involves several key steps:

Geostatic (Initial Step): In the initial step, We first remove the elements of the shield machine, the grouting layer and the segment, replace them with corresponding displacement boundary conditions, and carry out static analysis of the obtained model under the state of self-weight, so as to obtain a stress field result, and then assign the obtained stress field as the initial stress field to the original model for in-situ stress balance. In this way, the influence of the initial soil stress on the subsequent calculation results can be eliminated [22,23,24].

Initial Mud Support (N Analysis Step): In the N analysis step, we initiate the simulation by applying boundary conditions of mud pressure and pore pressure to the corresponding position of the palm surface, mimicking the mud support provided by the shield machine. This support pressure is continuously applied for one analysis step.

Soil Excavation (N+1 Analysis Step): In the N+1 analysis step, we replicate the excavation of soil as the shield machine advances.

Here, we employ the life-death unit method to deactivate the soil elements in front of the original palm face. The shield unit in front of the machine is activated, while the shield unit in the rear is deactivated. We apply the same mud pressure and pore pressure conditions to the next palm face to simulate the shield's progress. Additionally, we activate the grouting layer and segment units at this position and apply radial grouting pressure and pore pressure boundary conditions to simulate the grouting process at the shield tail.

Grout Hardening and Dissipation (N+6 Analysis Step): In the N+6 analysis step, we conclude the process by closing the boundary conditions of grouting pressure and pore pressure at this position. Furthermore, we enhance the modulus of the isoplasmic layer material to model grout hardening and grouting pressure dissipation.

These steps are cyclically executed to achieve dynamic tunnel shield excavation.

4.3 Calculation results and analysis

4.3.1 Model verification

In Figure 7, we compare the measured settlement curve with the calculated settlement curve of the embankment top following the shield tunneling through the levee. This visual representation allows us to assess the accuracy of our calculations and their compliance with specified requirements. The comparison reveals that the maximum calculated settlement value at the top of the levee, after the completion of the left hole shield tunnel, is 8.7mm. This value meets the specified requirements outlined in the project specifications. Furthermore, the calculated settlement curve closely aligns with the measured settlement curve, indicating a high level of accuracy in both our numerical calculation model and the associated processes outlined in this paper.
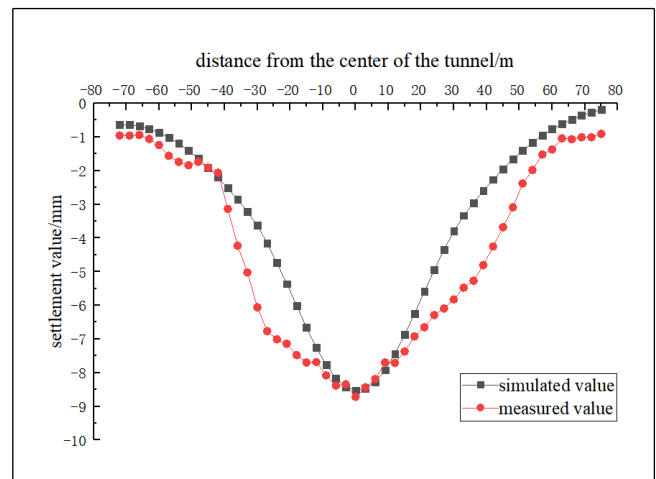

Figure 7. Measured settlement curve and calculated settlement curve of embankment top after shield tunneling through the levee

Figure 8 presents the calculated results of roof settlement in the levee during the penetration of the right-line shield. In the figure, the maximum measured settlement of the levee after the completion of the double-hole shield is 12.2mm. Importantly, this value aligns with the requirements specified in the project's specifications. While the calculated value is slightly smaller than the measured one, the agreement in the curve further substantiates the precision of our numerical calculation model.
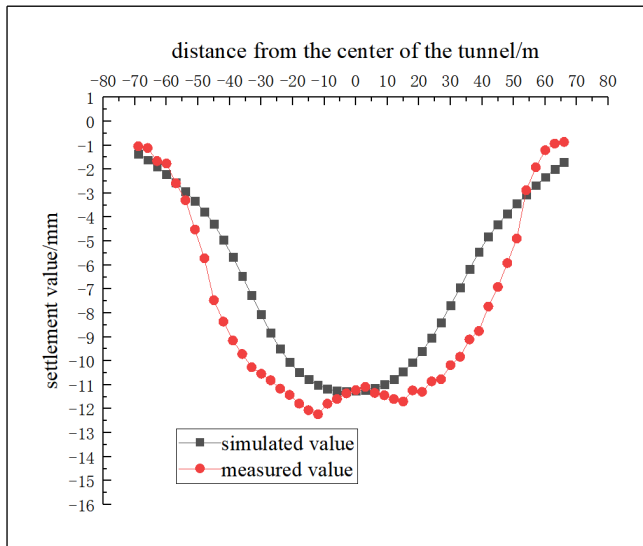
Figure 8. Calculation results of the roof settlement of the levee when the right line shield penetrates through the levee

Figure 9. Lateral settlement curve of soil at different depths of levee

Combined with Figure 3 and Figure 8, we analyze the factors contributing to the observed W-shaped settlement pattern. The settlement may be attributed to the following stages: 1) Before the shield arrives, the tunnel experiences overall subsidence due to the supporting pressure of the excavation face. 2) When the shield reaches the top of the left-line tunnel, the soil experiences unloading due to excavation and recovers elastic deformation, leading to a convex appearance at the top of the embankment. 3) As the shield progresses, the joint action of grouting pressure and other factors contributes to further settlement of the embankment top.

4.3.2 Deep soil settlement of levee

Figure 9 provides a comparative analysis of the lateral settling trough at the top of the levee and at depths of 10, 20, and 28 meters during the penetration of the left-line shield. The analysis reveals the following characteristics: 1) At varying depths, the transverse settlement trough exhibits a distinctive "V" shape, with the settling trough at the levee's summit showing a gentler slope. 2) Deeper depths show a slight increase in soil settlement above the tunnel axis and a simultaneous reduction in the width of the settlement trough. This phenomenon is attributed to stress redistribution in the surrounding soil as the shield traverses the levee, leading to the formation of a lateral settlement trough. 3) Stress propagation at the top of the levee is more dispersed, resulting in a less pronounced settlement effect. As depth increases, the soil above the tunnel axis bears a greater load, contributing to a slight rise in settlement, the narrowing of the settlement trough width is a consequence of the localized nature of stress transfer.

The characteristics of deep soil settlement of the levee bear some resemblance to those induced by the φ6.34m subway shield [25]. However, it is noteworthy that the maximum soil settlement experienced by the levee and the extent to which the width of the sedimentation tank varies with depth are significantly less pronounced compared to the subway shield. In light of these observations, it is reasonable to consider that, under the specific conditions of this project, the width coefficient (i_h) of the transverse sedimentation trough at varying depths closely approximates the width coefficient (i_0) of the s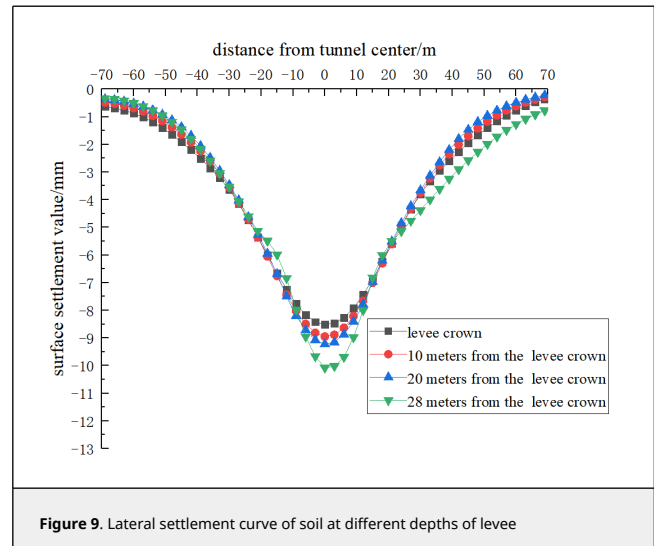urface transverse sedimentation trough. When a large-diameter shield passes through the levee, the disparity between the settlement value at the levee's crest and the settlement value in the corresponding deep soil strata appears to be minimal. This suggests that, in practical engineering applications, the settlement value recorded at the levee's surface can effectively serve as an indirect indicator of deep soil settlement. Consequently, there may be no compelling need for the specialized arrangement of deep settlement monitoring points unless exceptionally high precision is warranted.

Figure 10 presents a comparison of transverse settling troughs at various depths when the right-line shield passes through the levee. This analysis aims to shed light on the settlement patterns during this process. Upon examination, it's evident that the maximum settlement during the penetration of the right-line shield increases by 3.5 meters compared to the single-hole scenario. As we delve deeper into the analysis, several trends emerge: 1) With increasing depth, soil settlement above the tunnel axis experiences a slight increase. 2) The width of the sedimentation tank shows a minor decrease with depth. 3) Settlement in the shield area, overall, follows a "W" shape distribution.
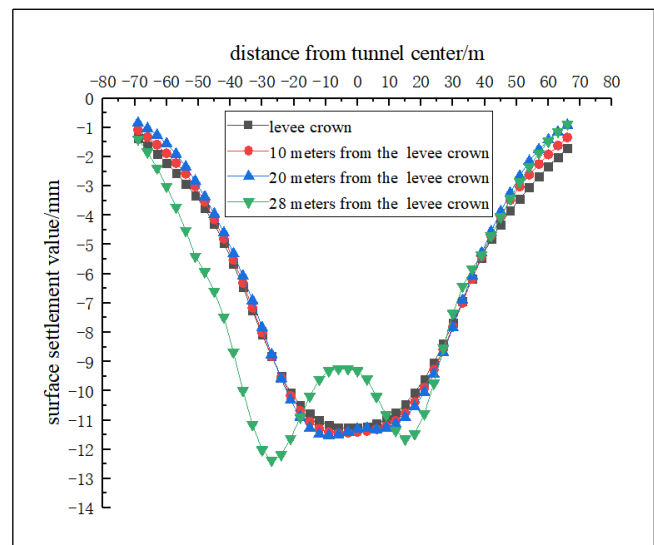

Figure 10. Lateral settling tank of soil in different depths of levee

![SCIPEDIA logo]

L. Zhongxiang, S. Lingchao, R. Abdullah, M. Shahrin, C. Yintao, S. Xin, F. Wenju, A. Islam and Z. Hengxu, Analysis of deformation of levee caused by large diameter shield tunneling in river crossing tunnel, Rev. int. métodos numér. cálc. diseño ing. (2024). Vol. 40, (1), 10

Notably, at a depth of 28 meters below the top of the embankment (coinciding with the grouting layer), there's a pronounced "W" shape settlement distribution. This phenomenon can be explained by two key factors:

1. The depth of 28 meters coincides with the shield construction area for the right-line, resulting in significant soil disturbance near the existing left line. This leads to soil redistribution and substantial settlement.
2. Additionally, this depth aligns with the grouting layer location. Typically, grouting processes enhance soil strength, potentially reducing interaction between soil masses. Consequently, the soil exhibits a marked "W" shape settlement distribution at the grouting layer depth.

In conclusion, this analysis reveals important settlement patterns during right-line shield penetration. These findings can have implications for future projects in similar conditions.

4.3.3 Horizontal displacement of deep soil mass of levee

Figure 11 displays the horizontal displacement curves of the soil mass at the top of the levee and at depths of 10, 20, and 28 meters during the penetration of the left-line shield. As seen from Figure 11, the horizontal displacement curve of the levee top exhibits an approximately inverted "S" shaped distribution, symmetrically centered around the tunnel axis. The horizontal displacement directly above the axis is zero, while the horizontal displacement on both sides of the axis is non-zero and directed towards the tunnel axis. The maximum horizontal displacement is 6.6 millimeters, with symmetry appearing at positions $\pm i$ from the tunnel axis.

1. At a depth of 10 meters from the top of the levee, the soil is situated in a shallower position, significantly affected by surface loads and shield construction. The mechanical compression from the shield and lateral soil displacement result in substantial soil deformation, leading to a reduction in horizontal displacement by approximately 42.4% compared to the top position of the embankment.
2. As the depth increases to 20 meters, the soil is positioned deeper, with reduced influence from surface loads and construction, resulting in minimal soil deformation and a relatively modest reduction in horizontal displacement of around 1 millimeter.
3. At a depth of 28 meters from the top of the embankment, the soil is deep and in proximity to the shield grouting layer. The maximum horizontal displacement occurs at positions ±0.5i, with a reverse bend point at the centerline of the tunnel. Despite minimal impact from surface loads, shield construction induces significant deformation due to the enhanced compressive strength of the soil from the grouting layer. This results in an asymmetric displacement distribution, with some soil moving towards the tunnel direction near the shield side and away from the grouting layer.

Figure 12 illustrates the horizontal displacement curves of the soil mass at the top of the levee and at depths of 10, 20, and 28 meters after shield tunneling. The horizontal displacement curve at the levee's crest exhibits an approximate "wave-like" distribution, symmetrically centered around the axis of the two tunnels. Above the axis, the horizontal displacement is zero, while on either side of the axis, it is non-zero and directed toward the tunnel axis. The maximum horizontal displacement recorded is 9.2 millimeters, symmetrically distributed at positions ±i from the tunnel axis. Distinct patterns in the
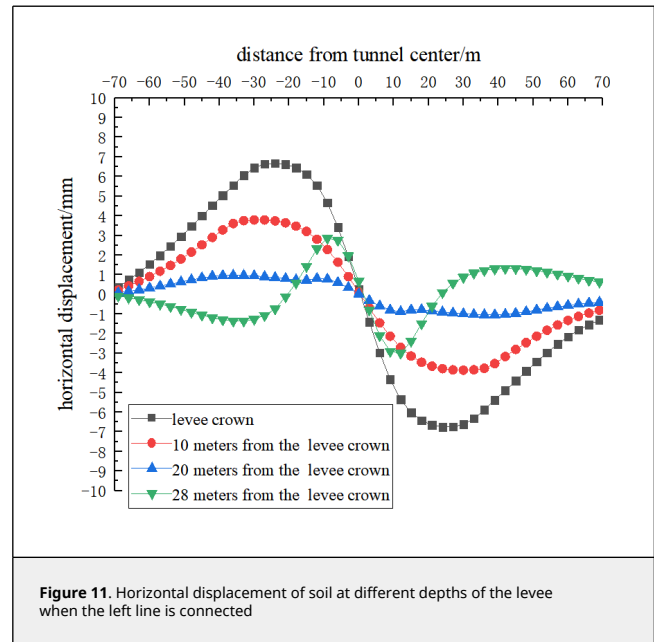

Figure 11. Horizontal displacement of soil at different depths of the levee when the left line is connected

variation of horizontal displacement become apparent at different depths:

1. At a depth of 10 meters, the soil experiences significant influences from surface loads and shield construction, resulting in substantial deformation and a reduction in maximum horizontal displacement by approximately 42.4% compared to the top position.
2. At 20 meters, with reduced influence from surface loads and construction, soil deformation decreases, leading to a relatively modest reduction in horizontal displacement of approximately 1 millimeter.
3. At 28 meters, coinciding with the shield grouting layer, the soil displays unique behavior, with maximum horizontal displacement observed directly above the tunnel's centerline. The presence of the grouting layer enhances the soil's compressive strength, causing asymmetric displacement distribution.

Real-time monitoring of horizontal displacement is crucial during the passage of a large-diameter shield tunnel, especially for deep soil layers within the levee. Additionally, when pile foundations or other retaining structures are present, proactive protective measures should be taken to anticipate additional shear forces and ensure levee safety.

5. Conclusions

1. When the left line shield penetrates through the levee, the maximum settlement of the top reaches 8.7mm, which meets the deformation control requirements. The surface transverse settlement trough is distributed in a "V" shape, and the width of the sedimentation trough on the top of the levee is about 5 times of the width coefficient of the sedimentation trough. The settlement distribution can be estimated by the Peck formula. When the levee is passed under the right line, the maximum settlement of the top reaches 12.2mm, which has a wider influence on the soil and a larger settlement.

2. When the left line shield tunneling underpasses the levee, the lateral settlement at different depths of the levee is distributed in a "V" shape, and the lateral settlement trough at the top of
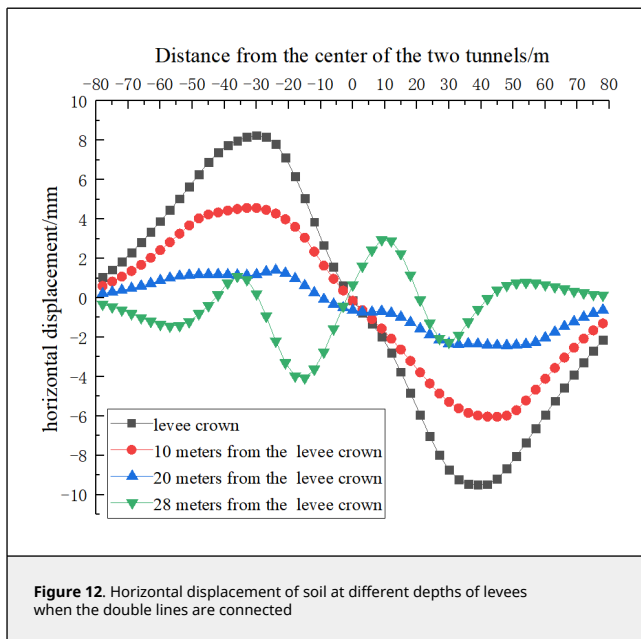
SCIPEDIA

L. Zhongxiang, S. Lingchao, R. Abdullah, M. Shahrin, C. Yintao, S. Xin, F. Wenju, A. Islam and Z. Hengxu, Analysis of
deformation of levee caused by large diameter shield tunneling in river crossing tunnel, Rev. int. métodos numér.
cálc. diseño ing. (2024). Vol. 40, (1), 10

Figure 12. Horizontal displacement of soil at different depths of levees when the double lines are connected

the levee is relatively gentle. With the increase of depth, the soil settlement above the tunnel axis slightly increases, while the width of the settlement trough slightly decreases. When the right line shield underpasses the levee, the lateral settlement at different depths of the levee shows a "W" shape distribution, and the "W" shape settlement of the soil at the depth of the grouting layer is more significant.

3. The horizontal displacement curves of the top of the levee and deep soil mass (except the grouting layer) are approximately inverted "S" shape when the left line shield underpasses the levee and the right line shield underpasses the levee, and the maximum horizontal displacement of the top of the levee and deep soil mass (except the grouting layer) occurs at the position of $\pm i$. And the maximum horizontal displacement of the right shield through the levee is greater than the maximum horizontal displacement of the left shield through the levee.

4. When the left line shield underpasses the levee, the maximum horizontal displacement at the grouting layer appears at the position of $\pm 0.5i$, and there is a reverse bending point at the center line of the tunnel. When the right line shield tunneling underpasses the levee, the maximum horizontal displacement at the grouting layer appears at the position of $\pm 0.5i$, and there are reverse bending points at the center line, $\pm i$ and $\pm 0.75i$ of the tunnel.

References

[1] Xie W., Wu W. Analysis of measured settlement of the Qiantang River embankment caused by under-crossing of large-diameter slurry shield tunneling. Modern Tunneling Technology, 48(4):142-147, 2011.

[2] Yang J. Finite difference analysis of impact of undercrossing super-large-diameter shield tunnel on training jetty. Chinese Journal of Geotechnical Engineering, 41(8):1569-1572, 2019.

[3] Zhang Y., Xia P., Zhu W., et al. Analysis of stratum deformation and stability: a case study of the Nanjing Weisan road river-crossing tunnel passing under the Yangtze River embankment. Modern Tunneling Technology, 52(4):151-157, 2015.

[4] Han L., Ye G., Wang J., et al. Finite element analysis of impact of under-crossing of large shallow shield tunnel on riverbank. Chinese Journal of Geotechnical Engineering, 37(S1):125-128, 2015.

[5] Li Z., Huang X. Study on settlement control for slurry shields crossing the embankment. Modern Tunneling Technology, 48(1):103-110, 2011.

[6] Zhang Z., Lin C., Wu S., et al. Analysis and control of ground settlement of embankments in construction of cross-river shield tunnels. Chinese Journal of Geotechnical Engineering, 33(6):977-984, 2011.

[7] Wu W., Sun Y., Li L. et al. Analysis of levee deformation caused by large diameter shield tunneling in river Crossing Tunnel. China Railway Science, 37(04):78-82, 2016.

[8] Huang H. Research on settlement of Qiantang River levee caused by large-diameter shield construction. Zhejiang, Zhejiang University of Technology, 2018.

[9] Zhu M., Wei L., Fang Y. et al. Study on settlement analysis and control of large diameter shield tunnel under the Yellow River levee. Modern Tunnel Technology, 59(03):211-219, 2022.

[10] Xie X., Yang C., Wang Q. et al. Settlement analysis and control study of shield crossing levee of Yangtze River in Nanjing and Yanlu River Crossing Passage. Chinese Journal of Rock Mechanics and Engineering, 40(S2):3313-3322, 2021.

[11] Lin Q., Cao P., Dong T. Numerical simulation of flood control levee deformation by shield tunnel excavation through the Liuyang River: A case study. Geofluids, 2023:156-163, 2023.

[12] Wu S., Lin C., Zhang Z., et al. Risk analysis and control for slurry shield under-passing embankment. Chinese Journal of Rock Mechanics and Engineering, 30(5):1034-1042, 2011.

[13] Epel T., Mooney M.A., Gutierrez N. The influence of face and shield annulus pressure on tunnel liner load development. Tunnelling and Underground Space Technology, 117, 104096, 2021.

[14] Lee H., Kwak J., Choi J., Hwang B., Choi H. A lab-scale experimental approach to evaluate rheological properties of foam-conditioned soil for EPB shield tunnelling. Tunnelling and Underground Space Technology, 128, 104667, 2022.

[15] Davoodi M., Senent S., Keshavarz A., Jimenez R. Three-dimensional seismic face stability of shield tunnels in undrained clay, Underground Space, 15:26-43, 2024.

[16] Zizka Z., Schoesser B., Thewes M. Investigations on transient support pressure transfer at the tunnel face during slurry shield drive part 1: Case A – Tool cutting depth exceeds shallow slurry penetration depth. Tunnelling and Underground Space Technology, 118, 104168, 2021.

[17] Zizka Z., Schoesser B., Thewes M. Investigations on the transient support pressure transfer at the tunnel face during slurry shield drive part 2: Case B – Deep slurry penetration exceeds tool cutting depth. Tunnelling and Underground Space Technology, 118, 104169, 2021.

[18] Seol H., Won D., Jang J., Yeom Kim K., Sup Yun T. Ground Collapse in EPB shield TBM site: A case study of railway tunnels in the deltaic region near Nak-Dong River in Korea. Tunnelling and Underground Space Technology, 120, 104274, 2022.

[19] Peck R.B. Deep excavations and tunneling in soft ground. State of the Art Report, Proceedings of 7th International Conference on Soil Mechanics and Foundation Engineering, Mexico City, 225-290, 1969.

[20] O'Reilly M.P., New B.M. Settlements above tunnels in the United Kingdom-their magnitude and prediction. Proc. Tunnelling 82, Institution of Mining and Metallurgy, London, 173-182, 1982.

[21] Jiang P.W., Zhang Z.H., Zheng H., et al. Coupling analysis method of grouting construction with deformation response of adjacent existing tunnel. Underground Space, 15:312-330, 2024.

[22] Abdellah W.R., Haridy A.K.A., Mohamed A.K., et al. Behaviour of horseshoe-shaped tunnel subjected to different in situ stress fields. Applied Sciences-Basel, 12(11), 5399, 2022.

[23] Nguyen T.T., Do N.A., Karasev M.A., et al. Influence of tunnel shape on tunnel lining behaviour. Proceedings of the Institution of Civil Engineers-Geotechnical Engineering, 174(4):355-371, 2021.

[24] Do N.A., Dias D., Zhang Z.X., et al. Study on the behavior of squared and sub-rectangular tunnels using the Hyperstatic Reaction Method. Transportation Geotechnics, 22, 100321, 2020.

[25] Sun Y., Zhou S., Gong Q. Distribution of deep displacement field during shield tunneling in soft-soil areas. Chinese Journal of Rock Mechanics and Engineering, 28(3):500-506, 2009.